CrystEngComm

PAPER

View Article Online
View Journal | View Issue

Cite this: *CrystEngComm*, 2015, **17**, 2974

Alkyl linker effects on the coordination topology of ditopic di(2-pyridylmethyl)amine carboxylate ligands with Zn^{II} and Cu^{II}: polymers *vs.* macrocycles†

Kiattipoom Rodpun,[a] Allan G. Blackman,[bc] Michael G. Gardiner,[d] Eng Wui Tan,[b] Carla J. Meledandri[a] and Nigel T. Lucas*[a]

Received 22nd February 2015,
Accepted 8th March 2015

DOI: 10.1039/c5ce00375j

www.rsc.org/crystengcomm

A series of ditopic ω-di(2-pyridylmethyl)amine carboxylic acid ligands incorporating a range of *n*-alkyl linkers (**C_nCOOH**, *n* = 3–5, 7, 10 and 11) have been synthesised. Solution phase studies showed a 1 : 1 coordination stoichiometry between the ligands and $M(ClO_4)_2{\cdot}6H_2O$ (M = Zn^{II} or Cu^{II}) in all cases. The Zn^{II} and Cu^{II} complexes were subsequently crystallised by liquid–liquid diffusion and the solid-state structures investigated by X-ray crystallography. The crystal structures obtained are entirely consistent with the 1 : 1 metal–ligand ratio of the solution-phase adducts. However, the coordination geometries and complex topologies are dependent on the alkyl chain length of the ligand **C_nCOOH**. The Zn^{II} and Cu^{II} complexes of the short alkyl chain ligands (*n* ≤ 5) exhibit 1D coordination polymeric structures with somewhat different conformations for $\{[Zn(\mathbf{C_3COO})(H_2O)](ClO_4){\cdot}3.5H_2O\}_n$ (**1**), $\{[Zn(\mathbf{C_4COO})(H_2O)]_4(ClO_4)_4{\cdot}1.5H_2O\}_n$ (**2**), $\{[Zn(\mathbf{C_5COO})(H_2O)](ClO_4)\}_n$ (**3**), $\{[Cu(\mathbf{C_3COO})](ClO_4){\cdot}MeOH\}_n$ (**4**), $\{[Cu(\mathbf{C_4COO})(H_2O)]_2(ClO_4)_2{\cdot}2H_2O\}_n$ (**5**) and $\{[Cu(\mathbf{C_5COO})(H_2O)](ClO_4){\cdot}2H_2O\}_n$ (**6**). In contrast, the ligands with longer alkyl chains (*n* ≥ 7) participate in Zn_2L_2 metallomacrocyclic structures $\{[Zn(\mathbf{C_7COO})(H_2O)](ClO_4)\}_2$ (**7**), $[Zn_2(\mathbf{C_{10}COO})_2(H_2O)_2](ClO_4)_2{\cdot}2H_2O{\cdot}MeOH$ (**8**) and $\{[Zn_2(\mathbf{C_{11}COO})_2(H_2O)_2][Zn_2(\mathbf{C_{11}COO})_2](ClO_4)_4{\cdot}H_2O\}_n$ (**9**). The formation of metallomacrocycles instead of the 1D coordination polymers is a persistent trend and, with identical crystal growth conditions and a non-coordinating anion employed, appears to be an effect of the longer alkyl chain.

Introduction

Crystal engineering of organic–inorganic hybrid architectures has attracted significant interest in recent years due to remarkable potential for application in materials science.[1] Specifically, coordination polymers generated by the self-assembly of multidentate ligands and transition metal ions has become the subject of particularly intriguing research, due in part to their convenient preparation and ease of structural modification.[2]

Careful ligand design facilitates the desired propagation of metal–ligand units in coordination polymers. In particular, a well-known strategy is to design a bridging ligand with terminal X-donor atoms (typically X = N, O, P, S).[3] Ditopic bridging ligands containing terminal pyridine or carboxylate groups have been widely utilised as good candidates for the construction of coordination polymers due to the efficient coordination abilities of their multiple donor moieties.[4] In addition, Cu^{II} and Zn^{II} ions are considered two of the most interesting divalent transition metals which can provide novel chemical and physical properties from a coordination perspective.[5] In light of the observations above, we have prepared a series of di(2-pyridylmethyl)amine-appended carboxylate ligands (Scheme 1) with an alkyl chain tether of variable length (*n* = 3–5, 7, 10, 11) as ligands to react with Cu^{II} and Zn^{II} ions. In addition, the metal–ligand coordination ratios have been investigated by solution studies prior to growing crystals for solid-state characterisation.

[a] *MacDiarmid Institute for Advanced Materials and Nanotechnology, Department of Chemistry, University of Otago, P.O. Box 56, Dunedin 9054, New Zealand. E-mail: nlucas@chemistry.otago.ac.nz*
[b] *Department of Chemistry, University of Otago, P.O. Box 56, Dunedin 9054, New Zealand*
[c] *School of Applied Sciences, Auckland University of Technology, Private Bag 92006, Auckland 1142, New Zealand*
[d] *School of Physical Sciences (Chemistry), University of Tasmania, Private Bag 75, Hobart 7001, Australia*

† Electronic supplementary information (ESI) available: CCDC 1037287–1037295. Mass spectrometry data and Job plots for M^{II}:**C_nCOOH** solutions, powder X-ray diffraction plots, details of variations to X-ray crystallographic procedures, tabulated bond lengths, angles and coordination geometries for **1**–**9**. For crystallographic data in CIF or other electronic format see DOI: 10.1039/c5ce00375j

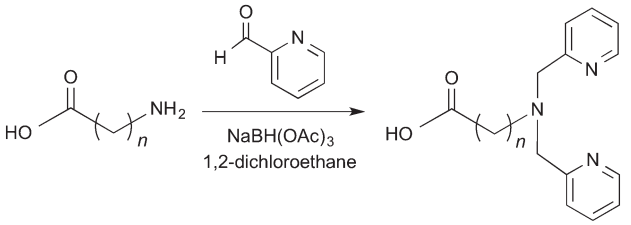

C_3COOH (n = 3)
C_4COOH (n = 4)
C_5COOH (n = 5)
C_7COOH (n = 7)
C_{10}COOH (n = 10)
C_{11}COOH (n = 11)

Scheme 1 General synthesis of di(2-pyridylmethyl)alkylamine-appended carboxylate ligands **C_nCOOH**.

In examining the solid-state coordination topology of the ligands by X-ray crystallography, particular attention can be focused on the effects of varying the chain length of the alkyl tether connecting the tertiary amine nitrogen atom and the carboxyl group. By keeping the metal–ligand ratio, the counteranion and the crystallisation solvent constant ensures that that the effect of the these parameters on the coordination topology is uniform.[6] As the size of the flexible alkyl linker is increased, greater conformational freedom allows for more structural possibilities but with a concomitant decrease in control of the ultimate product structure.

To date, the majority of coordination polymers utilising di(2-pyridylmethyl)alkylamine-appended carboxylate ligands have been reported to form one-dimensional (1D) structures.[7] Furthermore, it should be noted that within these reports, only ligands containing short carboxylate-pendant arms with an alkyl chain of five or fewer carbon atoms were employed.[8]

In the present study, Zn^{II} and Cu^{II} coordination complexes formed using di(2-pyridylmethyl)amine-appended carboxylate ligands (ligands denoted herein as **C_nCOOH**, as per Scheme 1) of **C_3COOH**, **C_4COOH** and **C_5COOH** are revisited with all solid-state structural determinations at low temperature (92–100 K). However, this work extends further to include an investigation of the effect of longer alkyl arms on the coordination behaviour of the ligands **C_7COOH**, **C_{10}COOH** and **C_{11}COOH**. The longer alkyl chain length ligands are more entropically unfavourable for coordination interactions[7] and ligand solubility is limited in the polar solvents most compatible with metal salt precursors.[9] Accordingly, the attainment of X-ray diffraction-quality crystals of complexes from long alkyl ligands is a challenging problem; nevertheless we report success in this endeavour. Moreover, our X-ray crystal structure data of these complexes reveals topological variation beyond the 1D chains observed for **C_3COOH**, **C_4COOH** and **C_5COOH**, in particular structures involving metallomacrocycles. Most ditopic ligands with flexible linkers that have previously been employed in studies of structurally diverse coordination architectures are symmetrical with identical functionality at both termini.[10] To the best of our knowledge, the metallomacrocycles reported herein are the first examples obtained from the use of bifunctional ditopic ligands with an alkyl chain of extended length, as distinct from macrocycles obtained from the use of symmetrical ligands with mono or bidentate termini.[11]

Experimental

Materials and methods

Unless otherwise stated, all reagents are commercially available and were used without further purification. Pyridine-2-carboxaldehyde was purchased from Alfa Aesar and further purified by short path distillation (80 °C) on a Kügelrohr before use. Elemental analyses were performed by the Campbell Microanalytical Laboratory, University of Otago; reported elemental percentages (C, H, N, Cl) are accurate to within ±0.4%. ^{1}H and ^{13}C NMR spectra were obtained at 25 °C on either a Varian 400-MR or Varian 500 MHz AR spectrometer. Chemical shifts are reported relative to solvent signals (^{1}H NMR: 7.26 ppm, ^{13}C NMR: 77.36 ppm). Electrospray mass spectrometry (ESI-MS) was carried out on a Bruker micrOTOF-Q in positive mode. Sampling was averaged for 2 min over a m/z range of 50 to 3000 amu. The mass was calibrated using sodium formate clusters, with 15 calibration points from 90 to 1050 amu, using a quadratic plus HPC line fit. ESI-MS spectra were processed using Compass software.[12] Infrared (IR) spectra were recorded on a Bruker Alpha FT-ATR IR spectrometer with a diamond anvil Alpha-P module.

General method for the preparation of ω-[di(2-pyridylmethyl) amino]alkanoic acid (C_nCOOH)

Pyridine-2-carboxaldehyde (2 mole equiv.) was added to a mixture of ω-aminoalkanoic acid (1 mole equiv.) and sodium triacetoxyborohydride (2.5 molar equiv.) in dichloroethane (20 mL). The suspension was stirred at room temperature for 12 h. The mixture was quenched with water, and chloroform (100 mL) was added. The organic layer was separated and dried over anhydrous Na_2SO_4. After removal of the solvent under reduced pressure, the residue was purified *via* column chromatography on silica (DCM/MeOH = 9 : 1) to obtain the desired product.

C_3COOH. Yield 69%. Anal. calcd for $C_{16}H_{19}N_3O_2$: C, 67.35; H, 6.71; N, 14.73%. Found: C, 67.52; H, 6.59; N, 14.94%. ^{1}H NMR ($CDCl_3$): δ 10.85 (1H, br), 8.54 (2H, d), 7.71 (2H, t), 7.46 (2H, d), 7.22 (2H, t), 3.86 (4H, s), 2.67 (2H, t), 2.35 (2H, t), 1.68–1.59 (2H, m). ^{13}C NMR ($CDCl_3$): δ 177.73, 156.59, 150.44, 145.78, 130.57, 128.73, 58.86, 56.38, 33.67, 24.51. MS (ESI): m/z calcd for $C_{16}H_{20}N_3O_2^+$ $[M + H]^+$ 286.1556, found 286.1539. Selected IR (ATR) ν/cm^{-1}: 2954 (m, C–H str), 1717 (s, C═O str), 1556 (m, C═N str), 756 (m), 447 (w).

C_4COOH. Yield 71%. Anal. calcd for $C_{17}H_{21}N_3O_2$: C, 68.20; H, 7.07; N, 14.04%. Found: C, 68.55; H, 7.35; N, 14.28%. ^{1}H NMR ($CDCl_3$): δ 10.77 (1H, br), 8.51 (2H, d), 7.64 (2H, t), 7.51 (2H, d), 7.13 (2H, t), 3.78 (4H, s), 2.54 (2H, t), 2.26 (2H, t), 1.66–1.57 (4H, m). ^{13}C NMR ($CDCl_3$): δ 177.63, 159.58, 149.27, 138.00, 125.24, 122.84, 59.95, 54.73, 35.08, 24.59, 24.25. MS (ESI): m/z calcd for $C_{17}H_{22}N_3O_2^+$ $[M + H]^+$ 300.1712, found

300.1701. Selected IR (ATR) ν/cm^{-1}: 2958 (m, C–H str), 1723 (s, C═O str), 1559 (m, C═N str), 756 (m), 449 (w).

C_5COOH. Yield 75%. Anal. calcd for $C_{18}H_{23}N_3O_2$: C, 68.98; H, 7.40; N, 13.41%. Found: C, 69.35; H, 7.65; N, 13.78%. ^{1}H NMR ($CDCl_3$): δ 10.30 (1H, br), 8.45 (2H, d), 7.56 (2H, t), 7.44 (2H, d), 7.04 (2H, t), 3.74 (4H, s), 2.44 (2H, t), 2.24 (2H, t), 1.651.52 (4H, m), 1.43–1.25 (2H, m). ^{13}C NMR ($CDCl_3$): δ 175.51, 159.57, 148.75, 136.53, 125.88, 122.59, 62.05, 57.05, 39.68, 27.29, 25.85, 24.76. MS (ESI): m/z calcd for $C_{18}H_{24}N_3O_2^+$ $[M + H]^+$ 314.1869, found 314.1853. Selected IR (ATR) ν/cm^{-1}: 2962 (m, C–H str), 1725 (s, C═O str), 1558 (m, C═N str), 760 (m), 447 (w).

C_7COOH. Yield 70%. Anal. calcd for $C_{20}H_{27}N_3O_2$: C, 70.35; H, 7.97; N, 12.31%. Found: C, 70.62; H, 8.49; N, 12.53%. ^{1}H NMR ($CDCl_3$): δ 10.28 (1H, br), 8.49 (2H, d), 7.60 (2H, t), 7.47 (2H, d), 7.11 (2H, t), 3.79 (4H, s), 2.55 (2H, t), 2.28 (2H, t), 1.70–1.54 (4H, m), 1.40–1.27 (6H, m). ^{13}C NMR ($CDCl_3$): δ 176.81, 160.70, 149.11, 137.71, 126.61, 123.24, 63.68, 57.33, 40.22, 29.92, 28.55, 27.72, 25.67, 24.79. MS (ESI): m/z calcd for $C_{20}H_{28}N_3O_2^+$ $[M + H]^+$ 342.2182, found 342.2169. Selected IR (ATR) ν/cm^{-1}: 2964 (m, C–H str), 1729 (s, C═O str), 1562 (m, C═N str), 763 (m), 451 (w).

C_{10}COOH. Yield 69%. Anal. calcd for $C_{23}H_{33}N_3O_2$: C, 72.03; H, 8.67; N, 10.96%. Found: C, 72.40; H, 8.92; N, 11.28%. ^{1}H NMR ($CDCl_3$): δ 10.22 (1H, br), 8.52 (2H, d), 7.63 (2H, t), 7.51 (2H, d), 7.12 (2H, t), 3.77 (4H, s), 2.59 (2H, t), 2.22 (2H, t), 1.61–1.51 (4H, m), 1.38–1.22 (12H, m). ^{13}C NMR ($CDCl_3$): δ 176.11, 161.33, 149.50, 138.63, 126.94, 124.45, 63.87, 57.42, 40.86, 38.12, 34.12, 33.64, 33.07, 29.55, 27.42, 25.67, 25.46. MS (ESI): m/z calcd for $C_{23}H_{34}N_3O_2^+$ $[M + H]^+$ 384.2651, found 384.2642. Selected IR (ATR) ν/cm^{-1}: selected IR (ATR) ν/cm^{-1}: 2966 (m, C–H str), 1732 (s, C═O str), 1563 (m, C═N str), 769 (m).

C_{11}COOH. Yield 68%. Anal. calcd for $C_{24}H_{35}N_3O_2$: C, 72.51; H, 8.87; N, 10.57%. Found: C, 72.85; H, 9.12; N, 10.88%. ^{1}H NMR ($CDCl_3$): δ 9.90 (1H, br), δ 8.55 (2H, d), 7.68 (2H, t), 7.56 (2H, d), 7.18 (2H, t), 3.82 (4H, s), 2.64 (2H, t), 2.33 (2H, t), 1.66–1.55 (4H, m), 1.41–1.27 (14H, m). ^{13}C NMR ($CDCl_3$): δ 175.16, 158.89, 148.95, 138.32, 127.16, 125.00, 64.79, 55.25, 39.60, 38.72, 35.85, 33.44, 32.97, 29.59, 29.52, 28.00, 26.77, 26.43. MS (ESI): m/z calcd for $C_{24}H_{36}N_3O_2^+$ $[M + H]^+$ 398.2808, found 398.2793. Selected IR (ATR) ν/cm^{-1}: 2968 (m, C–H str), 1735 (s, C═O str), 1566 (m, C═N str), 767 (m).

General method for solution studies of metal–ligand coordination stoichiometry by ESI-MS

M^{II} : C_nCOOH solutions (1 : 2 ratio). 100 μL of $M(ClO_4)_2{\cdot}6H_2O$ (M = Zn^{2+} or Cu^{2+}, 0.030 M) in H_2O was added to 100 μL of 0.060 M ω-di(2-pyridylmethyl)aminoalkanoic acid (C_nCOOH, n = 3–5, 7, 10 and 11) in MeOH. The mixtures were diluted with 1 mL of MeOH and ESI-MS data were collected immediately in order to observe the equilibrium metal–ligand coordination stoichiometry in solution (details in Table S1†).

M^{II} : C_nCOOH solutions (1 : 1 ratio). Solutions (1 : 1 ratio) were prepared similarly to those used for the 1 : 2 ratio, except 0.060 M $M(ClO_4)_2{\cdot}6H_2O$ was used.

M^{II} : C_nCOOH solutions (2 : 1 ratio). Solutions (2 : 1 ratio) were prepared similarly to those used for the 1 : 2 ratio, except 0.0600 M $M(ClO_4)_2{\cdot}6H_2O$ and 0.030 M C_nCOOH were used.

Job's method of continuous variations

100 mL stock solutions of 0.010 M C_nCOOH (n = 3–5, 7, 10 and 11) in 0.100 M $HClO_4$ and 0.010 M $Cu(ClO_4)_2{\cdot}6H_2O$ in 0.100 M $HClO_4$ were prepared. These solutions were used to prepare mixtures with systematically varied mole fractions of the ligand and metal (details in Table S2†). The absorbances of these solutions were measured at 650 nm and plotted against mole fraction of the ligand C_nCOOH.

General synthesis of coordination polymers/macrocycles from C_nCOOH

$M(ClO_4)_2{\cdot}6H_2O$ (M = Zn^{2+} or Cu^{2+}, 0.100 mmol) was dissolved in water (2.0 mL) and carefully layered with a methanolic solution of C_nCOOH (0.100 mmol in 2.5 mL). Crystals suitable for X-ray analysis were obtained within 2 days and were isolated, dried in air and weighed.

$\{[Zn(C_3COO)(H_2O)][ClO_4){\cdot}3.5H_2O\}_n$ (1). Yield 71%. Anal. calcd for $C_{16}H_{24}ClN_3O_9Zn$: C, 38.19; H, 4.81; N, 8.35; Cl, 7.04%. Found: C, 38.33; H, 4.67; N, 8.52; Cl, 6.84%. Selected IR (ATR) ν/cm^{-1}: 2963 (m, C–H str), 1722 (m, C═O str), 1563 (m, C═N str), 1072 (s, ClO_4^-), 762 (m).

$\{[Zn(C_4COO)(H_2O)]_4(ClO_4)_4{\cdot}1.5H_2O\}_n$ (2). Yield 67%. Anal. calcd for $C_{68}H_{91}Cl_4N_{12}O_{29.50}Zn_4$: C, 41.84; H, 4.70; N, 8.61; Cl, 7.26%. Found: C, 41.75; H, 5.01; N, 8.34; Cl, 6.91%. Selected IR (ATR) ν/cm^{-1}: 2968 (m, C–H str), 1728 (m, C═O str), 1566 (m, C═N str), 1075 (s, ClO_4^-), 764 (m).

$\{[Zn(C_5COO)(H_2O)][ClO_4)\}_n$ (3). Yield 70%. Anal. calcd for $C_{18}H_{24}ClN_3O_7Zn$: C, 43.66; H, 4.88; N, 8.49; Cl, 7.16%. Found: C, 43.82; H, 4.75; N, 8.33; Cl, 7.23%. Selected IR (ATR) ν/cm^{-1}: 2967 (m, C–H str), 1728 (m, C═O str), 1566 (m, C═N str), 1078 (s, ClO_4^-), 766 (m).

$\{[Cu(C_3COO)][ClO_4){\cdot}MeOH\}_n$ (4). Yield 63%. Anal. calcd for $C_{17}H_{22}ClCuN_3O_7$: C, 42.59; H, 4.63; N, 8.77; Cl, 7.40%. Found: C, 42.75; H, 4.72; N, 8.69; Cl, 7.22%. Selected IR (ATR) ν/cm^{-1}: 2965 (m, C–H str), 1724 (m, C═O str), 1563 (m, C═N str), 1074 (s, ClO_4^-), 764 (m).

$\{[Cu(C_4COO)(H_2O)]_2(ClO_4)_2\}_n$ (5). Yield 64%. Anal. calcd for $C_{34}H_{44}Cl_2Cu_2N_6O_{14}$: C, 42.59; H, 4.63; N, 8.77; Cl, 7.40%. Found: C, 42.88; H, 4.80; N, 8.82; Cl, 7.53%. Selected IR (ATR) ν/cm^{-1}: 2966 (m, C–H str), 1728 (m, C═O str), 1565 (m, C═N str), 1077 (s, ClO_4^-), 765 (m).

$\{[Cu(C_5COO)(H_2O)][ClO_4){\cdot}2H_2O\}_n$ (6). Yield 66%. Anal. calcd for $C_{18}H_{28}ClCuN_3O_9$: C, 40.84; H, 5.33; N, 7.94; Cl, 6.70%. Found: C, 40.80; H, 5.46; N, 8.07; Cl, 6.73%. Selected IR (ATR) ν/cm^{-1}: 2968 (m, C–H str), 1728 (m, C═O str), 1565 (m, C═N str), 1076 (s, ClO_4^-), 765 (m).

$\{[Zn(C_7COO)(H_2O)][ClO_4)\}_2$ (7). Yield 58%. Anal. calcd for $C_{40}H_{56}Cl_2N_6O_{14}Zn_2$: C, 45.91; H, 5.39; N, 8.03; Cl, 6.77%. Found: C, 46.12; H, 5.48; N, 7.87; Cl, 6.52%. Selected IR

(ATR) ν/cm^{-1}: 2972 (m, C–H str), 1732 (m, C═O str), 1569 (m, C═N str), 1078 (s, ClO_4^-), 767 (m).

$[Zn_2(C_{10}COO)_2(H_2O)_2](ClO_4)_2{\cdot}2H_2O{\cdot}MeOH$ (8). Yield 61%. Anal. calcd for $C_{47}H_{76}Cl_2N_6O_{17}Zn_2$: C, 47.09; H, 6.39; N, 7.01; Cl, 5.91%. Found: C, 47.13; H, 6.44; N, 6.89; Cl, 5.78%. Selected IR (ATR) ν/cm^{-1}: 2976 (m, C–H str), 1735 (m, C═O str), 1571 (m, C═N str), 1080 (s, ClO_4^-), 769 (m).

$[Zn_2(C_{11}COO)_2(H_2O)_2](ClO_4)\{[Zn_2(C_{11}COO)_2](ClO_4)_4{\cdot}H_2O\}_n$ (9). Yield 54%. Anal. calcd for $C_{96}H_{142}Cl_4N_{12}O_{27}Zn_4$: C, 50.14; H, 6.22; N, 7.31; Cl, 6.17%. Found: C, 50.29; H, 6.37; N, 7.20; Cl, 6.33%. Selected IR (ATR) ν/cm^{-1}: 2979 (m, C–H str), 1737 (m, C═O str), 1572 (m, C═N str), 1082 (s, ClO_4^-), 771 (m).

X-ray crystal structure determinations

Crystallographic data collection, processing and refinement details for **1–9** are reported in Table 1. Data were collected on either a Bruker Kappa APEXII diffractometer (sealed tube Mo,

Table 1 Summary of crystallographic data for **1–9**

	1	2	3	4	5
Formula	$C_{16}H_{27}ClN_3O_{10.5}Zn$	$C_{68}H_{91}Cl_4N_{12}O_{29.5}Zn_4$	$C_{18}H_{24}ClN_3O_7Zn$	$C_{17}H_{22}ClCuN_3O_7$	$C_{34}H_{48}Cl_2Cu_2N_6O_{16}$
M	530.23	1951.81	495.22	479.37	994.76
Radiation	Mo Kα	Cu Kα	Mo Kα	Mo Kα	Cu Kα
T (K)	92(2)	100(1)	93(2)	100(1)	100(1)
Crystal system	Monoclinic	Orthorhombic	Orthorhombic	Monoclinic	Orthorhombic
Space group	$P2_1/n$	$Pna2_1$	$Pbca$	$P2_1/n$	$Pna2_1$
a (Å)	9.0642(10)	17.5644(3)	15.7557(10)	10.3751(3)	14.1032(2)
b (Å)	19.594(2)	34.1856(4)	15.1427(9)	8.3150(3)	17.7710(2)
c (Å)	12.6956(15)	13.3561(2)	16.8380(10)	23.5131(11)	15.8877(2)
α (°)	90	90	90	90	90
β (°)	104.058(6)	90	90	102.275(4)	90
γ (°)	90	90	90	90	90
V (Å^3)	2187.2(4)	8019.7(2)	4017.3(4)	1982.08(13)	3981.90(9)
Z	4	4	8	4	4
Crystal size (mm)	0.44 × 0.20 × 0.06	0.18 × 0.13 × 0.08	0.55 × 0.42 × 0.35	0.44 × 0.09 × 0.03	0.30 × 0.15 × 0.10
μ (mm^{-1})	1.306	3.359	1.403	1.282	3.256
θ_{min}, θ_{max} (°)	2.4979, 30.3364	3.31, 76.63	2.74, 30.54	3.151, 28.423	3.73, 74.16
Reflections measured	38 578	55 998	86 630	19 827	16 054
Independent reflections	6661	14 452	6140	4477	6950
Parameters/restraints	379/249	1115/902	277/3	270/161	598/105
R_1 [$I > 2\sigma(I)$]	0.0592	0.0626	0.0309	0.0562	0.0564
wR_2[$I > 2\sigma(I)$]	0.1410	0.1652	0.0806	0.1456	0.1542
GOF	1.177	1.033	1.033	1.072	1.045
Residual extrema (e Å^{-3})	−0.815, 0.869	−0.983, 2.217	−0.467, 0.527	−1.214, 1.256	−1.004, 0.797
Flack parameter		0.00(13)			0.49(3)

	6	7	8	9
Formula	$C_{18}H_{28}ClCuN_3O_9$	$C_{20}H_{28}ClN_3O_7Zn$	$C_{47}H_{76}Cl_2N_6O_{17}Zn_2$	$C_{96}H_{142}Cl_4N_{12}O_{27}Zn_4$
M	529.42	523.27	1198.78	2299.50
Radiation	Mo Kα	Cu Kα	Mo Kα	Synchrotron
T (K)	100(1)	100(1)	93(2)	100(2)
Crystal system	Orthorhombic	Tetragonal	Triclinic	Monoclinic
Space group	$Pca2_1$	$I4_1/a$	$P\bar{1}$	Cc
a (Å)	13.0446(3)	16.9390(2)	9.4210(17)	36.788(7)
b (Å)	8.8181(2)	16.9390(2)	22.221(5)	8.669(2)
c (Å)	19.3686(5)	33.5981(6)	29.851(7)	33.481(7)
α (°)	90	90	110.023(13)	90
β (°)	90	90	90.136(13)	102.29(3)
γ (°)	90	90	97.835(12)	90
V (Å^3)	2227.94(9)	9640.3(2)	5809(2)	10 433(4)
Z	4	16	4	4
Crystal size (mm)	0.60 × 0.43 × 0.22	0.34 × 0.24 × 0.24	0.36 × 0.13 × 0.10	0.20 × 0.03 × 0.03
μ (mm^{-1})	1.155	2.820	0.987	1.091
θ_{min}, θ_{max} (°)	3.886, 28.758	4.73, 74.85	0.73, 22.56	1.17, 25.03
Reflections measured	20 122	18 903	35 674	81 232
Independent reflections	4893	4814	15 134	17 724
Parameters/restraints	295/121	467/569	1164/1281	1304/56
R_1 [$I > 2\sigma(I)$]	0.0468	0.0863	0.1558	0.0452
wR_2[$I > 2\sigma(I)$]	0.1173	0.2575	0.3696	0.1154
GOF	1.023	1.064	1.016	1.040
Residual extrema (e Å^{-3})	−0.537, 0.972	−0.999, 0.819	−0.749, 3.341	−0.857, 0.994
Flack parameter	0.009(19)			0.0(4)

graphite monochromated; **1**, **3**, **8**); an Agilent SuperNova with Atlas CCD using mirror monochromated micro-focus Mo or Cu-Kα radiation (**2**, **4**–**7**); or at the MX2 beamline of the Australian Synchrotron (λ = 0.7180 Å; **9**).[13] The data processing was undertaken with SAINT and XPREP[14] (**1**, **3**, **8**), CrysAlisPro[15] (**2**, **4**–**7**) or XDS[16] (**9**), and included a numerical or analytical[17] absorption correction over a face-indexed model and/or a multiscan empirical correction, except the data for **9** which was not corrected for absorption. All structures were solved by direct methods with SHELXS-97 (ref. 18) (**1**–**5**, **8**–**9**), Superflip[19] (**6**) or SIR-97 (ref. 20) (**7**) and were extended and refined against all F^2 data with SHELXL-97 (ref. 18) using the X-Seed[21] interface. The non-hydrogen atoms in the asymmetric unit were modelled with anisotropic displacement parameters. Hydrogen atoms were placed in calculated positions and refined using a riding model with fixed C–H distances (sp^2-CH 0.95 Å, sp^3-CH_3 0.98 Å, sp^3-CH_2 0.99 Å) and isotropic displacement parameters estimated as $U_{iso}(H)$ = $1.2U_{eq}(C)$, except for CH_3 where $U_{iso}(H)$ = $1.5U_{eq}(C)$. Where significant residual electron density peaks were observed, oxygen-bound hydrogen atoms were included and refined with O–H restraints (0.84 Å) and $U_{iso}(H)$ = $1.5U_{eq}(O)$. Special conditions/variations to the general procedure are given in the ESI.†

Powder X-ray diffraction

Crystals were dried, ground to a fine powder and data collected at room temperature with Cu-Kα radiation (λ = 1.5418 Å) on a PANalytical X'Pert-Pro MPD PW3040/60 XRD with Rapid RTMS X'Celerator Detector in the Department of Geology, University of Otago. The samples were scanned at 40 kV and 30 mA from 3–80° 2θ using a step size of 0.0080° and a scan step time of 4.03 s. Data were collected and processed using PANanalytical HighScore Plus, Version 4.

Results and discussion

Preparation of ω-[di(2-pyridylmethyl)amino]alkanoic acid ligands (C_nCOOH)

A homologous series of the ligands **C_nCOOH** has been prepared according to a literature procedure with minor modifications.[22] The general reductive amination synthetic approach employed in the syntheses involves Schiff base formation between the primary amine group of the aminoalkanoic acid and the aldehyde group of pyridine-2-carboxaldehyde, and subsequent reduction of the resulting imine. This method gave the desired products as pale yellow oils in good yields (68–75%) and employs milder conditions than dialkylation of an aminoalkanoic acid with 2-picolyl chloride hydrochloride which requires heating at reflux, as described in alternative procedures.[8a–d]

Solution studies of metal–ligand coordination stoichiometry

High resolution ESI-MS was used to investigate the metal–ligand coordination stoichiometry of Zn^{II} or Cu^{II} with the **C_nCOOH** ligands in solution.[23] In particular, the ratio of metal ion to ligand in solution was varied between 1 : 2, 1 : 1 to 2 : 1, and freshly-prepared solutions were subsequently analysed. Despite different ratios of the metal ion and ligand being used, ESI-MS data in all cases presented similar mass distributions with matching isotopic patterns. The major signal essentially corresponds to a singly-charged ion assigned to metal–carboxylate $[M(C_nCOO)]^+$ as the only significant peak, with good agreement between the experimental and calculated *m*/*z* values and isotopic pattern. This suggests that a 1 : 1 coordination stoichiometry is preferred for the complexation and does not depend upon the metal–ligand ratio in solution or length of the alkyl linker. The mass spectrometry data of the metal–ligand solutions with different ratios are listed in Table S1.† Note that $[M(C_nCOO)]^+$ can arise from 1 : 1 metal–ligand polymeric structures in the solid-state. However, polymeric species are typically not detected by ESI-MS due to low stability, although steric constraints caused by the poly-methylene linkers while in solution may also be a factor.[9]

The method of continuous variation (Job's method) was also used to determine the stoichiometry of the reactants at chemical equilibrium.[24] In order to confirm the metal–ligand ratios, plots of absorbance *vs.* mole fraction of **C_nCOOH** in solutions with Cu^{II} are shown in Fig. S2.† As is seen for all cases, the plots exhibit a maximum absorbance at a 0.5 mole fraction of **C_nCOOH**. Therefore, the derived stoichiometric ratios of the complexes in solution are 1 : 1 in all cases.[24b] The results from the Job method agree well with the results from solution studies by ESI-MS, which also suggest a 1 : 1 stoichiometry for the most stable species, irrespective of the molar ratios used.

Synthesis of coordination polymers/macrocycles from C_nCOOH

In accordance with the 1 : 1 metal–ligand complex stoichiometries which were identified from the solution studies by ESI-MS and Job's method, possible linear/macrocyclic coordination structures are shown in Fig. 1.

To investigate the actual coordination structures in the solid-state, a 1 : 1 metal–**C_nCOOH** ratio was subsequently applied to grow crystals of Zn^{II} and Cu^{II} complexes. Slow diffusion of a methanolic solution of **C_nCOOH** into an aqueous solution of $M(ClO_4)_2{\cdot}6H_2O$ (M = Zn^{II} or Cu^{II}) afforded colourless and blue crystalline solids, respectively. Infrared spectral data of the complexes show evidence of coordination of the ligand **C_nCOOH** by their carboxylate group. All the free ligands display strong absorption bands in the range 1723–1735 cm^{-1} which are assigned to ν(C=O) of the carboxyl group. However, the decreasing intensity of these C=O bands which are observed as medium bands in the spectra of their complexes, indicate that C=O stretching vibration is reduced due to the carboxylate oxygen atoms being coordinated to the metal ions.[25]

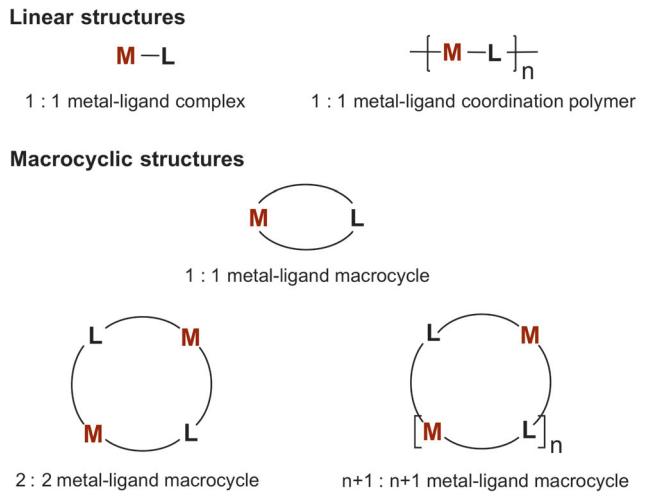

Fig. 1 Potential coordination structures for a 1:1 coordination stoichiometry of $[M(C_nCOO)]^+$.

X-ray crystal structures

Zn^{II} coordination polymers (1–3). $\{[Zn(C_3COO)(H_2O)](ClO_4)\cdot 3.5H_2O\}_n$ (**1**) was found to crystallise in the monoclinic space group $P2_1/n$. The asymmetric unit contains one $[Zn(C_3COO)(H_2O)]^+$ unit, one perchlorate anion and disordered lattice water. The coordination environment around the Zn^{II} metal centre is ZnN_3O_2. As shown in Fig. 2a, the central Zn^{II} is ligated by three nitrogen donors of one ligand molecule and one carboxylate oxygen atom from the adjacent ligand. The penta-coordination is completed through ligation by an aqua ligand. The $[Zn(C_3COO)(H_2O)]^+$ units are linked by the ditopic coordination of C_3COO^- to form a 1D coordination polymer with an intrapolymer Zn···Zn separation of 6.8563(9) Å. It is interesting to note that the second carboxylate oxygen (O2) does not coordinate to the Zn^{II} metal centre but participates in a hydrogen bond with a Zn^{II}-bound water (O3···O2 2.683(3), O3–H31···O2 1.86(3) Å; Fig. 3). The polymeric chain has a wave topology due to the intramolecular hydrogen bonds described above, supported by an intermolecular hydrogen bond chain between the second aqua ligand hydrogen (H32), lattice water molecules O91, O92 and the Zn-bound carboxylate oxygen O1 (Fig. 3).

The Zn^{II}-tertiary amine bond distance (Zn1–N3 2.170(3) Å) is longer than the analogous bond distances involving the pyridyl nitrogen atoms (Zn1–N1 2.111(3), Zn1–N2 2.109(3) Å). The N1–Zn–N3 and N2–Zn–N3 bite angles of the five-membered chelate rings are 79.09(11)° and 79.19(11)°, respectively. According to Addison *et al.*,[26] an index of geometry (τ) of 0 and 1 are identified as ideal square pyramidal and trigonal bipyramidal geometries, respectively. The Zn^{II} centre of **1** displays a distorted square pyramidal geometry (τ = 0.10) which is similar in geometry to a previously reported structure involving the same ligand and metal.[8e] As evidence of phase purity, powder X-ray diffraction measurements (Cu-Kα, room temperature) from crystals of **1** (also for **3**, **4**, **6**) are shown in Fig. S2–S5;† insufficient material was available for powder diffraction studies on the other complexes.

$\{[Zn(C_4COO)(H_2O)]_4(ClO_4)_4\cdot 1.5H_2O\}_n$ (**2**) also has 1D polymeric chain structure (Fig. 2b). The coordination polymer **2**, crystallises in the orthorhombic space group $Pna2_1$, and the asymmetric unit consists of four independent $[Zn(C_4COO)(H_2O)]^+$ units connected together, along with four perchlorate anions, and one and a half water molecules. The coordination environment of each Zn^{II} metal centre is ZnN_3O_3 with a distorted octahedral geometry. The apical positions are occupied by the two pyridyl nitrogen atoms, while the tertiary

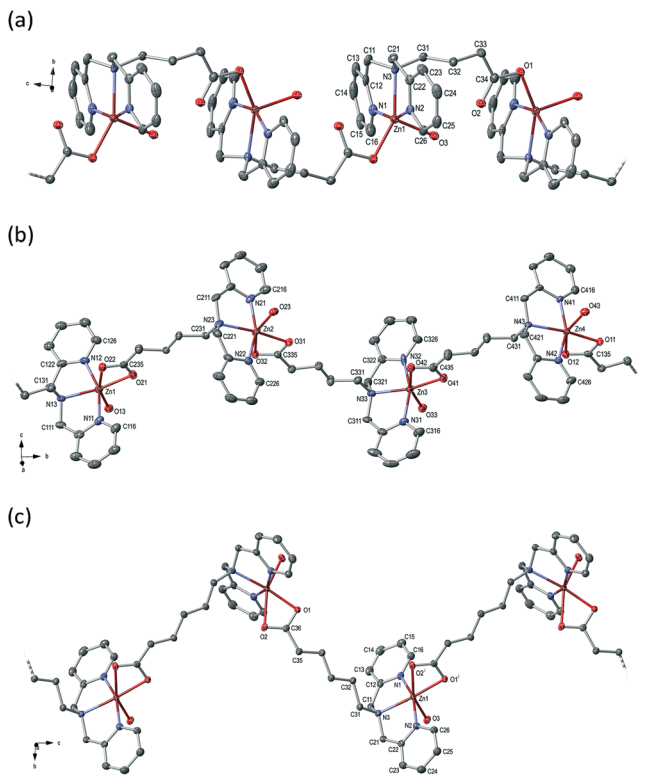

Fig. 2 ORTEP diagrams of the Zn^{II} coordination polymers (a) **1** (n = 3), (b) **2**, (n = 4), and (c) **3** (n = 5). All hydrogen atoms, perchlorate anions and solvent have been omitted for clarity. For bond lengths, angles and coordination geometries see Table S3.† Symmetry code: (i) x, 1/2 − y, 1/2 + z.

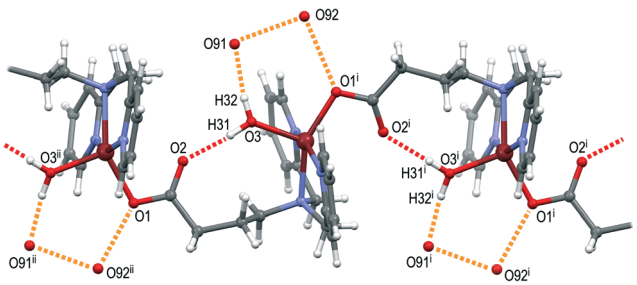

Fig. 3 Detail of hydrogen bonding interactions for **1**. Intramolecular H-bonding interactions are shown in red and intermolecular interactions in orange; O3···O2 2.683(3), O3···O91 2.703(8), O91···O92 2.649(8), O92···O1^i 2.823(5) Å. Symmetry codes: (i) 1/2 + x, 1/2 − y, 1/2 + z; (ii) −1/2 + x, 1/2 − y, −1/2 + z.

nitrogen, the aqua ligand and the neighbouring carboxylate oxygen atoms coordinate to the central Zn^{II} in the equatorial plane. The asymmetric unit repeats itself in a head-to-tail arrangement with intramolecular Zn···Zn distances of 9.848(2), 10.132(2), 10.063(2), 10.196(2) Å.

The 1D polymeric chain structure and carboxylate ligand binding mode of $\{[Zn(C_5COO)(H_2O)](ClO_4)\}_n$ (**3**) is similar to **2**, as illustrated in Fig. 2c. The coordination polymer **3** crystallises in the orthorhombic space group *Pbca*. The asymmetric unit contains one $[Zn(C_5COO)(H_2O)]^+$ unit accompanied by one perchlorate counterion but no solvent. The Zn^{II} metal centre also adopts a distorted octahedral ZnN_3O_3 coordination environment through bonding to three nitrogen donors of one ligand, two oxygen atoms from the neighbouring carboxylate bridge and a metal bound water. A similar crystal structure, prepared in refluxing water followed by recrystallization from acetonitrile/water, was studied at room temperature.[8d]

Cu^{II} coordination polymers (4–6). For the X-ray crystal structures of the Zn^{II} complexes derived from the short alkyl chain length ligands (C_nCOOH, $n \leq 5$), only 1D coordination polymeric chains are observed. To compare this behaviour with the analogous Cu^{II} complexes, their crystal structures were also investigated. The Cu^{II} complexes also provide 1D coordination polymers, albeit with an intriguing carboxylate coordination mode in the structure containing C_3COO^-.

$\{[Cu(C_3COO)](ClO_4)\cdot MeOH\}_n$ (**4**) crystallises in the monoclinic space group $P2_1/n$, and the asymmetric unit contains one Cu^{II} metal centre, carboxylate ligand, a perchlorate counterion, and a lattice methanol. As shown in Fig. 4a and 5a, each Cu^{II} exhibits a CuN_3O_3 coordination environment; the Cu^{II} centre is coordinated by three nitrogen donor atoms and one carboxylate oxygen atom (O2) from the same ligand. The remaining two coordination sites are occupied by both oxygen atoms belonging to the carboxylate group of the neighbouring ligand. Consequently, one {CuOCO} ring, two five-membered chelate rings of {CuNCCN} and a seven-membered $\{CuN(CH_2)_3CO\}$ ring are generated in this configuration. Of the chelate Cu–O bonds of the carboxylate bridge, one (Cu1–$O1^i$ 1.982(2) Å) has a bond length which is comparable to those of the Zn^{II} coordination polymers, whereas the remaining bond (Cu1–$O2^i$ 2.622(2) Å) is significantly longer.

Polymer **4** is dissimilar to all the Zn^{II} polymers **1**–**3** in that the carboxylate ligand folds back in a "scorpion-like"[6c] fashion, giving rise to mini cyclic subunits along the polymeric chain; the carboxylate 'tail' exhibits a short O2–Cu1 bond (2.181(3) Å) to the same metal chelated by the N_3 head group (Fig. 5a). Furthermore, the carboxylate oxygen atom O2 bridges a neighbouring Cu^{II} metal centre through a long Cu1–O2 bond (2.622(2) Å) and occupying the sixth coordination site of the Cu^{II} ion. Overall, the ligand can be described as a tetradentate ligand toward one Cu^{II} metal centre and as a bidentate ligand toward an adjacent metal centre forming a dense 1D polymeric chain with an intramolecular Cu···Cu distance of 4.4251(7) Å, significantly shorter than the Zn···Zn distance (6.8563(9) Å) in **1**.

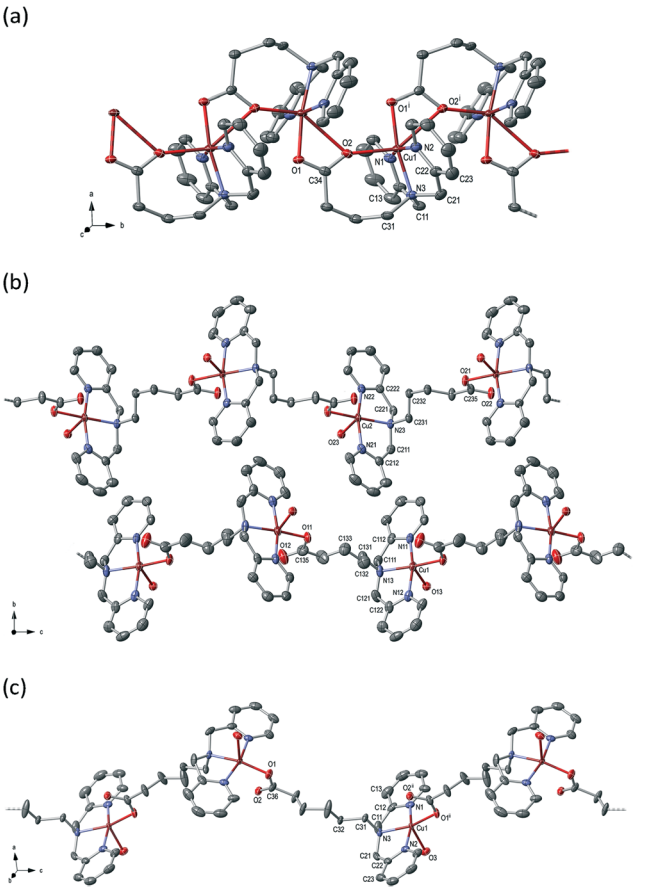

Fig. 4 ORTEP diagrams of the Cu^{II} coordination polymers (a) **4**, (b) **5**, and (c) **6**. All hydrogen atoms, perchlorate anions and solvent have been omitted for clarity. For bond lengths, angles and coordination geometries see Table S4.† Symmetry codes: (i) 3/2 − *x*, 1/2 + *y*, 1/2 − *z*; (ii) 1 − *x*, 1/2 − *y*, 1/2 + *z*.

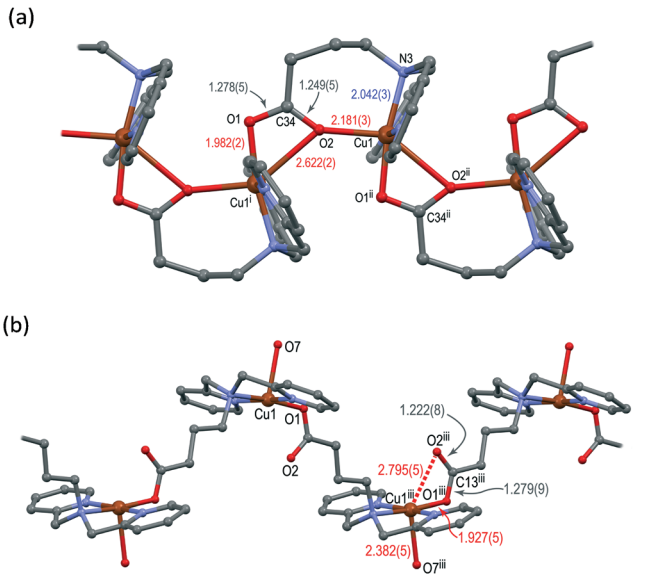

Fig. 5 Detail of the bonding of the carboxylate groups of (a) **4** (n = 3) and (b) a related Cu(II) structure of the same ligand (CSD code: EYEHAR).[8c] Hydrogen atoms, perchlorate anions and solvent molecules omitted for clarity. Symmetry codes: (i) 3/2 − *x*, −1/2 + *y*, 1/2 − *z*; (ii) 3/2 − *x*, 1/2 + *y*, 1/2 − *z*; (iii) 3/2 − *x*, −1/2 + *y*, 1/2 + *z*.

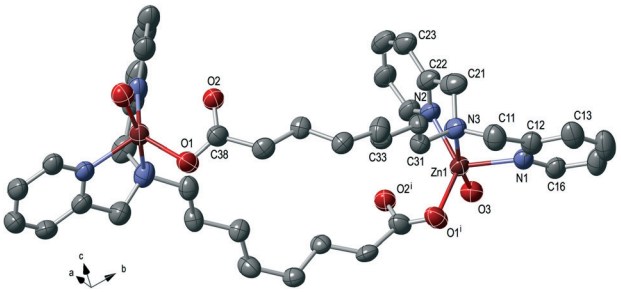

Fig. 6 ORTEP diagram of the Zn^{II} macrocycle **7** (symmetry expanded about a 2-fold axis). Minor disordered components of the alkyl chain, all hydrogen atoms and perchlorate anions have been omitted for clarity. Selected bond lengths, angles and the coordination geometries are listed in Table S5.† Symmetry code: (i) $1 - x, 1/2 - y, z$.

The hexa-coordinated Cu^{II} metal centre of **4** can be considered as having a distorted octahedral geometry (Fig. 5a), which is significantly different to the previously reported penta-coordinate $\{[Cu(C_3COO)(H_2O)](ClO_4)\cdot 3H_2O\}_n$.[8c] In this polymer the carboxylate group is monodentate and an aqua ligand occupies the axial site of a distorted square pyramid, resulting in a more open zig-zag polymer (Cu···Cu 9.370(1) Å) with a greater similar in topology to the Zn^{II} polymers **1–3** than **4**. The coordination geometry of these two structures is likely to be influenced by the crystallisation solvent and/or temperature; structure **4** (from methanol/water at room temperature) contains a lattice methanol, while $\{[Cu(C_3COO)(H_2O)](ClO_4)\cdot 3H_2O\}_n$ was recrystallised from hot water/acetonitrile and contains three lattice water molecules that participate in extensive hydrogen bonding.[8c]

$\{[Cu(C_4COO)(H_2O)]_2(ClO_4)_2\cdot 2H_2O\}_n$ (**5**) crystallised in the orthorhombic space group $Pna2_1$. The asymmetric unit contains two crystallographically-independent 1D polymeric chains of $\{[Cu(C_4COO)(H_2O)](ClO_4)\cdot 2H_2O\}_n$ aligned parallel to each other with opposing orientations (Fig. 4b). For each chain the three nitrogen atoms of the di(2-pyridylmethyl)-amine terminus coordinate to one copper site, while the oxygen atoms of each carboxylate terminus coordinate unsymmetrically to an adjacent site, giving rise to the 1D connectivity.

The CuN_3O_3 coordination geometry of each Cu^{II} centre is distorted octahedral wherein the axial positions are occupied by two pyridyl nitrogen atoms, while the equatorial positions are occupied by the tertiary nitrogen, a water molecule and both of the carboxylate oxygen atoms from the adjacent ligand. The structure is related to those previously described for penta-[8b] and hexa-[8a] coordinated structures, differing in the metal geometry and the identity of the counterion, respectively.

The polymer $\{[Cu(C_5COO)(H_2O)](ClO_4)\cdot 2H_2O\}_n$ (**6**) was found to crystallise in the orthorhombic space group $Pca2_1$. The asymmetric unit is composed of similar components as observed for **5**, albeit with C_5COO^- in the place of C_4COO^-. The CuN_3O_3 coordination environment of the Cu^{II} metal centre is best described as possessing a distorted octahedral

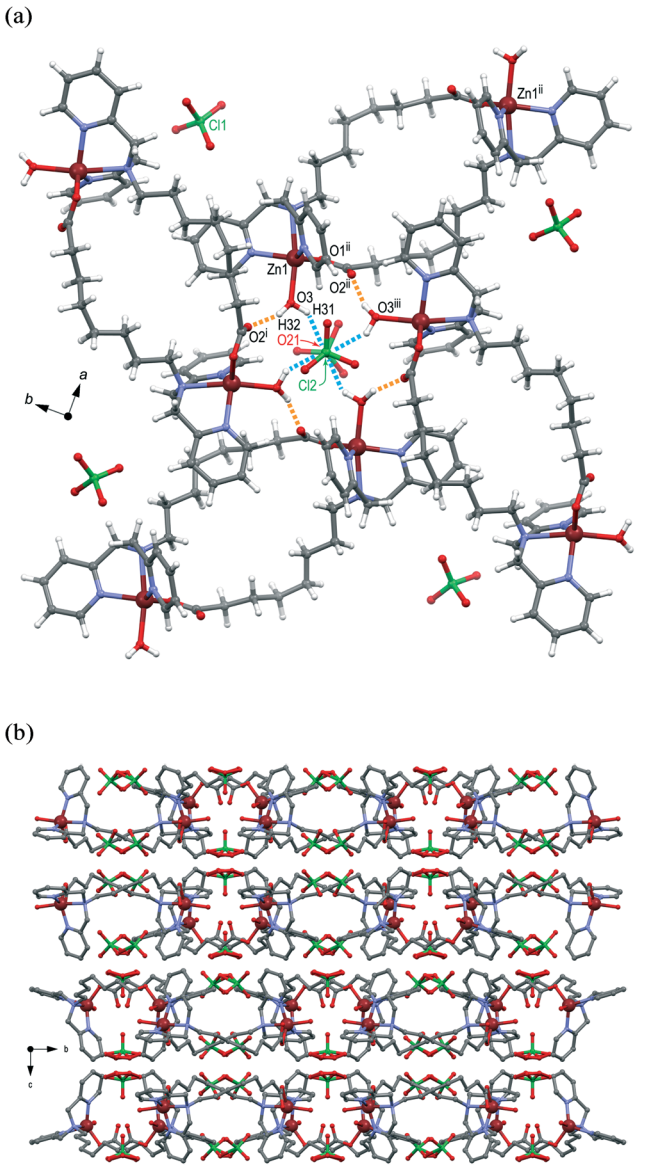

Fig. 7 Packing diagram of the Zn^{II} macrocycle **7** (n = 7) (a) viewed down the c-axis. Intermolecular H-bonding interactions at the inversion centre involve the aqua ligand hydrogens and a neighbouring carboxylate carbonyl oxygen (O3–H32···$O2^i$ 1.79(6), O3···$O2^i$ 2.597(6) Å; dashed orange lines) and perchlorate oxygen (O3–H31···O21 2.26(6), O3···O21 2.964(2) Å; dashed blue lines), (b) viewed down the a-axis showing the layered structure. Disordered perchlorate anions are shown in all possible sites. Symmetry codes: (i) $y - 1/4, 5/2 - x, 1/4 - z$; (ii) $1 - x, 1/2 - y, z$; (iii) $y - 1/4, 1/4 - x, 1/4 - z$.

geometry. The 1D zig-zag chain structure is shown in Fig. 4c. Another structure of Cu^{II} with C_5COOH has previously been reported but with a different geometry, namely a distorted square-pyramid around the Cu^{II} metal centre for crystals obtained from hot water/acetonitrile.[8b]

Based on these low temperature structural studies of the Zn^{II} and Cu^{II} complexes of the short chain ligands (C_nCOOH, $n \leq 5$), all are 1D coordination polymers with a similar coordination mode. Notably, an interesting difference in the

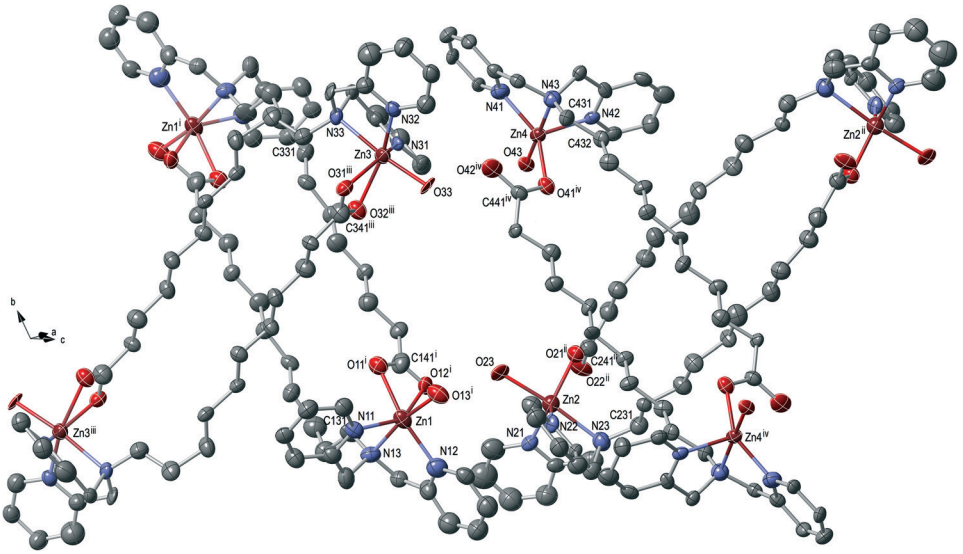

Fig. 8 ORTEP diagram of the Zn^{II} macrocycles **8** with 40% displacement ellipsoids. All hydrogen atoms, perchlorate anions and solvent have been omitted for clarity. For bond lengths, angles and coordination geometries see Table S5.† Symmetry codes: (i) 1 − *x*, 1 − *y*, −*z*; (ii) 2 − *x*, 1 − *y*, 1 − *z*; (iii) −*x*, 1 − *y*, −*z*; (iv) 1 − *x*, 1 − *y*, 1 − *z*.

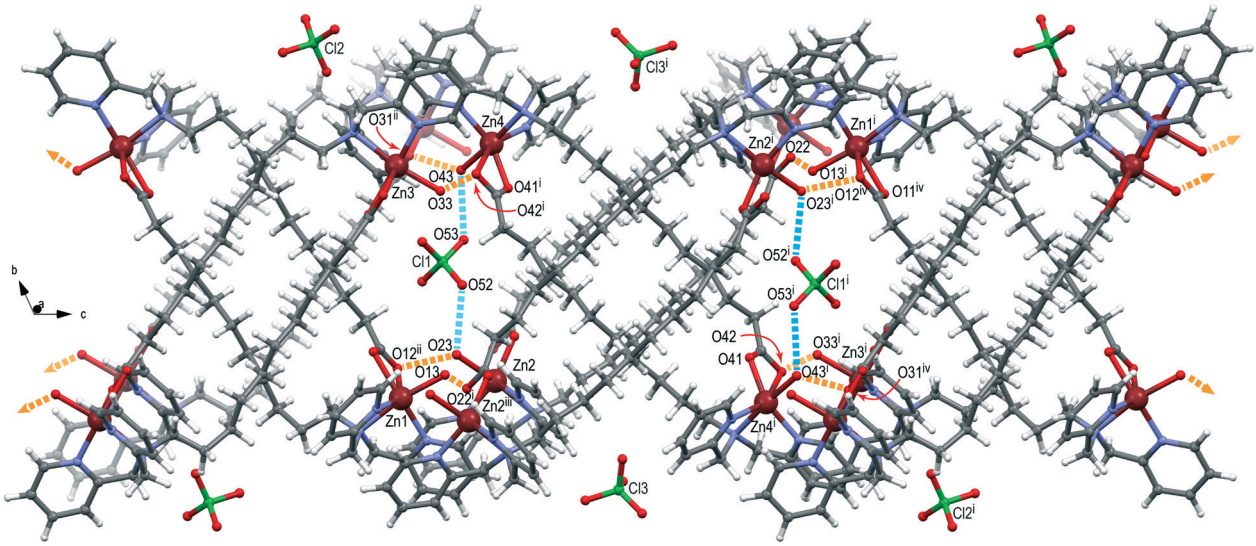

Fig. 9 Packing diagram of the Zn^{II} macrocycles **8** viewed down the *a*-axis showing intermolecular H-bonding interactions involving the aqua ligands and a neighbouring carboxylate oxygens (dashed orange lines) and perchlorate oxygen atoms (dashed light blue lines). Not all perchlorate anions and disordered solvent could be located in the model. Symmetry codes: (i) 1 − *x*, 1 − *y*, 1 − *z*; (ii) 1 − *x*, 1 − *y*, −*z*; (iii) *x* − 1, *y*, *z*; (iv) *x*, *y*, 1 + *z*.

carboxylate bonding in the Zn^{II} and Cu^{II} coordination polymers of the short C_3**COOH** ligand has been observed. An intramolecular H-bonding interaction folds the alkyl chain back in the Zn example, whereas the carboxylate coordinates back to the same metal ligated by the bis(pyridylmethyl)-amine in the Cu^{II} complex. The latter could be described as a "scorpion-like" coordination mode of the short ditopic ligand.

Zn^{II} macrocycles (7–9). In contrast to the polymeric Zn^{II} complexes of the short chain ligands (C_n**COOH**, $n \leq 5$), the structures with the longer analogues C_7**COOH**, C_{10}**COOH** and C_{11}**COOH** are dominated by metallomacrocycles. Moreover, the coordination geometry of the tridentate di(2-pyridylmethyl)amine moiety adjusts to facilitate macrocycle formation. Efforts to grow X-ray quality crystals of Cu^{II} complexes with the longer alkyl chain ligands proved unsuccessful and only the Zn^{II} complexes are reported herein.

The crystal structure of $\{[Zn(C_7COO)(H_2O)](ClO_4)\}_2$ (**7**) reveals the formation of a dimetallic M_2L_2 macrocycle (Fig. 6). The complex crystallises in the tetragonal space group $I4_1/a$. The asymmetric unit contains half of the macrocycle **7** with the other half generated by a 2-fold rotation about the

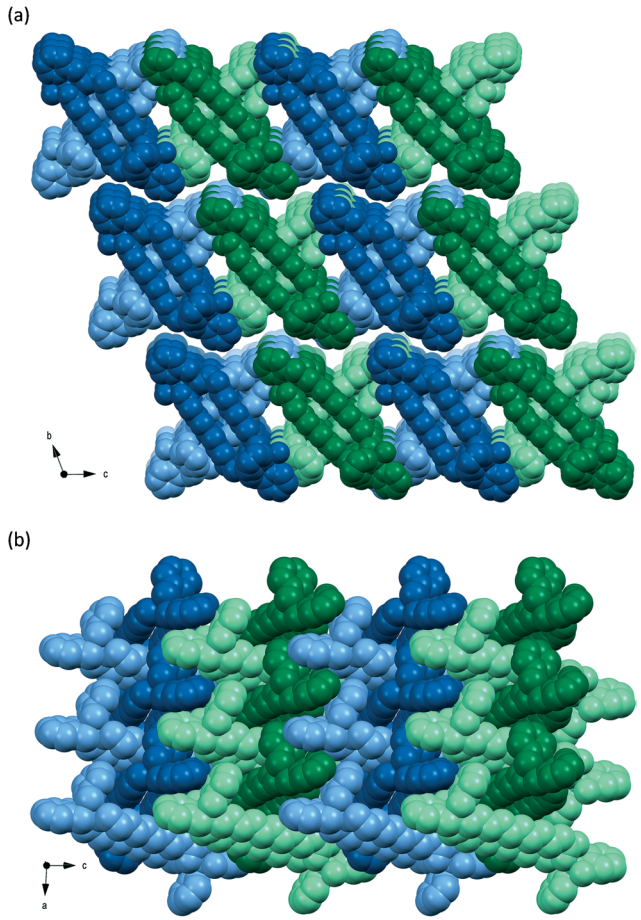

Fig. 10 Packing diagram of the Zn^{II} macrocycles **8** (a) viewed down the *a*-axis and (b) *b*-axis with each crystallographically independent macrocycle shown in a different colour (Zn1 blue, Zn2 light green, Zn3 light blue, Zn4 green). The perchlorate anions and disordered solvent are omitted for clarity.

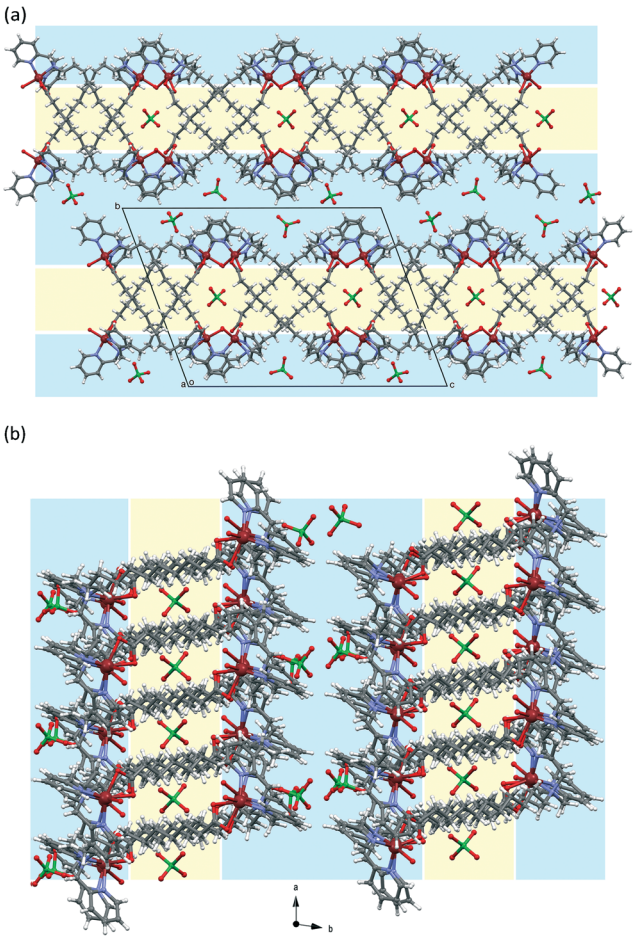

Fig. 11 Packing diagram of the Zn^{II} macrocycles **8** (a) viewed down the *a*-axis and (b) *c*-axis showing the nanosegregation of the aromatic (blue highlight) and aliphatic (yellow highlight) components of the ligands. Not all perchlorate anions and disordered solvent could be located in the model.

centre of the macrocycle. Each Zn^{II} metal atom is coordinated by three nitrogen atoms of one ligand, a carboxylate oxygen from the second ligand and an aqua ligand. Each pentacoordinate Zn^{II} centre displays a distorted trigonal bipyrimidal geometry (τ = 0.63) such that the nitrogen donor atoms are in a facial (*fac*) coordination mode with the amine nitrogen (N3) in an axial site. The *fac*-N_3 coordination here contrasts with a meridional geometry for the shorter alkyl chain coordination polymers. The Zn^{II} centres, linked by two bridging ligands, have a Zn···Zn separation of 11.853(1) Å.

As is seen for the polymers **1**–**3**, hydrogen bonds involving the aqua ligand are important interactions driving the molecular packing. Fig. 7a shows a four molecule motif at an inversion centre of the structure **7** where each aqua ligand acts as a double hydrogen bond donor. A non-ligating carbonyl oxygen from a neighbouring macrocycle points toward the water as a hydrogen bond acceptor of H32, an interaction that is repeated fourfold about the *c*-axis (dashed orange line, Fig. 7a). These are relatively strong interactions[27] with O3–H32···O2 1.79(6), O3···O2 2.597(6) Å. The second hydrogen of each water ligand is donated to one of two perchlorate anion sites (Cl2, disordered) that sit above and below the plane defined by the macrocycles (dashed blue lines, Fig. 7a); these

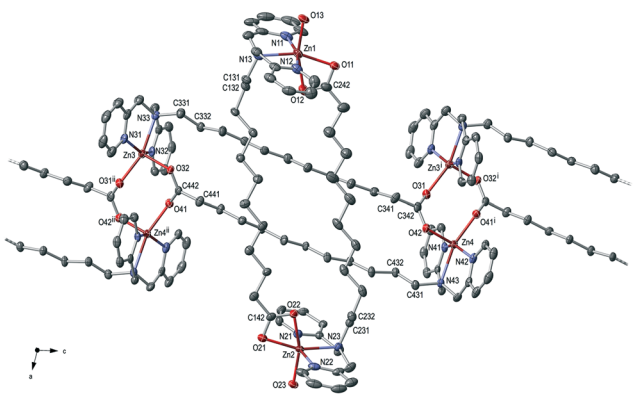

Fig. 12 ORTEP diagram of the Zn^{II} macrocycle and polymer **9**. All hydrogen atoms, perchlorate anions and solvent have been omitted for clarity. For bond lengths, angles and coordination geometries see Table S5.† Symmetry codes: (i) *x*, 1 − *y*, 1/2 + *z*; (ii) *x*, 1 − *y*, *z* − 1/2.

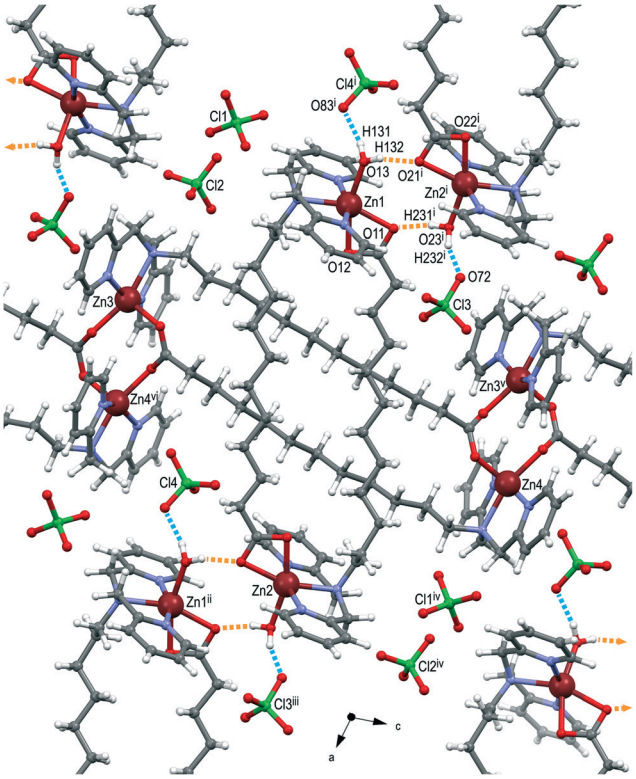

Fig. 13 Packing diagram of the **9** viewed down the *b*-axis onto the layers of interlocked Zn^{II} macrocycles and polymers. Second component of the disordered perchlorate anion at Cl1 has been omitted for clarity. Pairwise intermolecular H-bonding interactions between the discrete macrocycles (Zn1, Zn2) involve aqua ligand hydrogen atoms and a neighbouring carboxylate carbonyl oxygen (O13–H132···O21^{i} 1.86(5), O13···O21^{i} 2.669(5) Å and O23^{i}–H231^{i}···O11 1.82(4), O23^{i}···O11 2.650(5) Å; dashed orange lines); the second aqua hydrogen interacts with a perchlorate oxygen (O13–H131···O83^{i} 2.04(4), O13···O83^{i} 2.862(5) Å and O23^{i}–H232^{i}···O72 2.08(4), O23^{i}···O72 2.869(5) Å; dashed blue lines). Symmetry codes: (i) $x - 1/2, y - 1/2, z$; (ii) $1/2 + x, 1/2 + y, z$; (iii) $1/2 + x, y - 1/2, z$; (iv) $1/2 + x, 1/2 - y, 1/2 + z$; (v) $x, 1 - y, 1/2 + z$; (vi) $x, 1 - y, z - 1/2$.

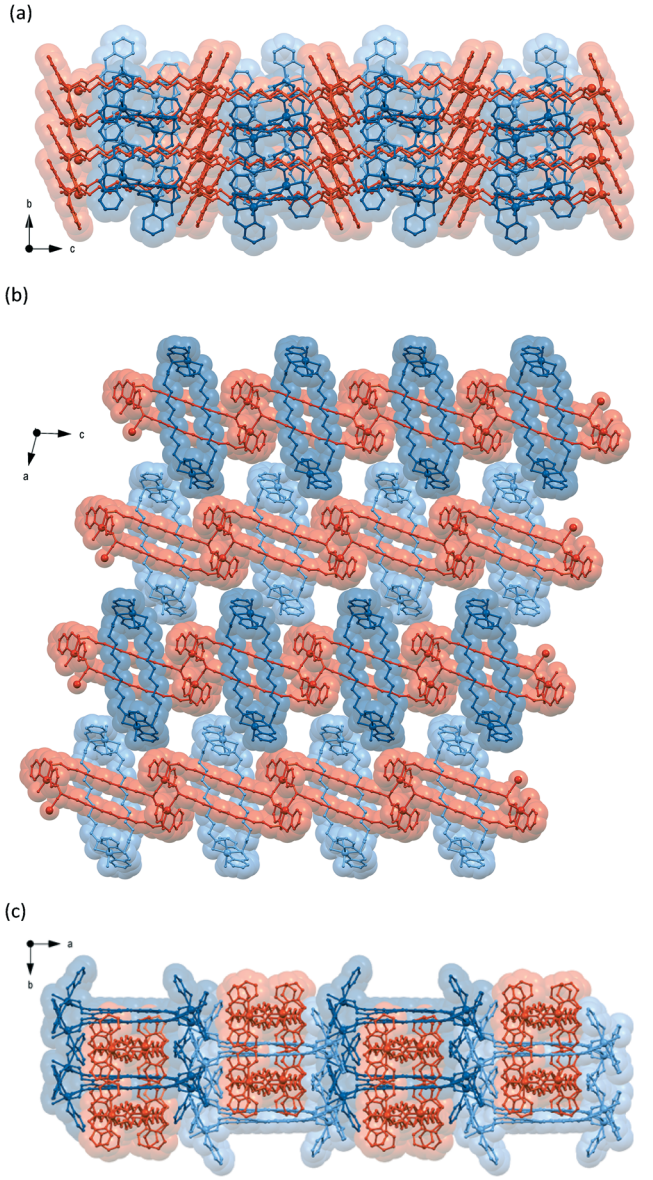

Fig. 14 Packing diagrams of Zn^{II} macrocyclic (blue) and polymer (red) components of **9** viewed along (a) the *a*-axis, (b) the *b*-axis, and (c) the *c*-axis. The perchlorate anions and water solvent have been omitted for clarity.

are weaker interactions, O3–H31···O21 2.26(6), O3···O21 2.964(2) Å, but act cooperatively. A second region of disordered perchlorate anions (Cl1) is adjacent to the alkyl chains (Cl1). The hydrogen-bond directed packing extends in the *ab*-plane to give layers of macrocycles that stack along the *c*-axis (Fig. 7b).

$[Zn_2(\mathbf{C_{10}COO})_2(H_2O)_2](ClO_4)_2{\cdot}2H_2O{\cdot}MeOH$ (**8**) was obtained from the crystallization of the $\mathbf{C_{10}COOH}$ ligand with $Zn(ClO_4)_2{\cdot}6H_2O$. The small crystals diffracted weakly and the low resolution data (*P*-1) were heavily restrained during refinement. Nevertheless, the data were sufficient to reveal an asymmetric unit containing four half macrocycles (Zn1–Zn4), each lying about an independent inversion centre, as well as one unit-occupancy and two half-occupancy perchlorate anions. The remaining contents of the asymmetric unit ($2ClO_4^-$, $4H_2O$, 2MeOH) are highly disordered and could not be modelled, their contribution accounted for using SQUEEZE.[28] The electron count and volume of the voids are consistent with the missing anions and solvent combination given above, supported by elemental analysis of crystals grown under the same conditions. Each macrocycle has the dimetallic formulation $[Zn_2(\mathbf{C_{10}COO})_2(H_2O)_2]^{2+}$ with a similar head-to-tail bridging coordination at Zn^{II} as for the macrocycle 7 (Fig. 8). The Zn^{II} ions display a distorted octahedral geometry in two out of four macrocycles, while the Zn^{II} ions of the remaining macrocycles exhibit a highly distorted square pyramidal geometry (τ = 0.49 Zn2, 0.44 Zn4) tending towards octahedral with a weak carboxylate O···Zn interaction; the N_3 donor atoms adopt a *fac*-coordination in all cases.

Examination of the packing shows again that hydrogen bonding with the water ligands dominate the intermolecular

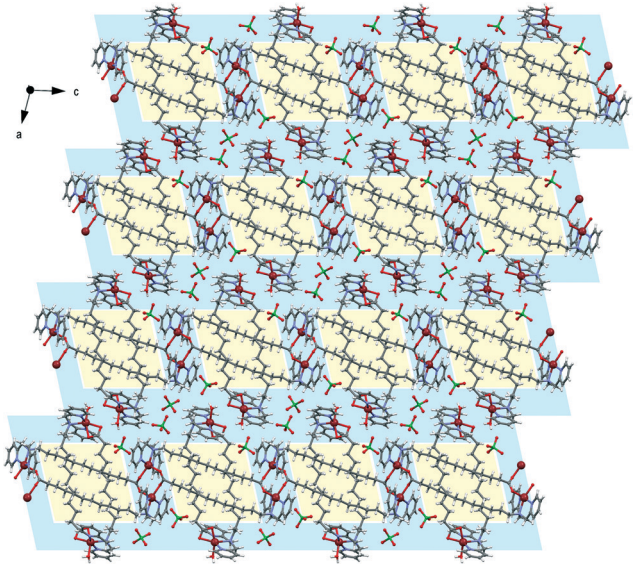

Fig. 15 Packing diagram of the Zn^{II} macrocycle and polymer **9** viewed down the *b*-axis showing the nanosegregation of the aromatic (blue highlight) and aliphatic (yellow highlight) components of the ligands, extending into the page along the *b*-axis. The second component of the disordered perchlorate anions and lattice water have been omitted for clarity.

interactions (Fig. 9). In particular, the complexes are arranged in a crossed fashion that places the metal centres in close proximity; this allows each Zn-bound water to interact with a neighbouring complex giving rise to a chain of hydrogen bonds that zig-zag along the *a*-axis. In addition, a perchlorate anion located in the void adjacent to the metals weakly hydrogen bonds to aqua ligands at Zn2 and Zn4. The elongated macrocycles stack along the *a*-axis in an alternating, criss-crossed arrangement (Fig. 10) with a separation of *ca.* 4.71 Å. There are two crystallographically-independent columns (blue and green in Fig. 10) that interlock at the ligated metal regions, stabilised through hydrogen bonding (as discussed above) and aromatic embrace motifs[29] involving both edge-to-face and offset face-to-face π–π interactions of the pyridyl rings. The interlocking of the macrocycle columns along the *c*-axis gives sheets with cationic metal centres at the interface and regularly packed alkyl chains sandwiched at the centre; this arrangement has similarities with the arrangement of charged surfactant molecules in bilayer structures. The counteranions here are mostly located at the interface between the layers, although as shown in Fig. 9, a small channel of *ca.* 3 Å running parallel to the column axis accommodates anions (and solvent), stabilised through hydrogen bonding. Fig. 11 further emphasises the nanosegregation of the metal centres, surrounded by aromatic-rich groups (blue highlight), from the densely packed aliphatic regions (yellow highlight).

Crystallization of $Zn(ClO_4)_2{\cdot}6H_2O$ with the longer $C_{11}COOH$ ligand affords the monoclinic (*Cc*) structure $\{[Zn_2(C_{11}COO)_2(H_2O)_2][Zn_2(C_{11}COO)_2](ClO_4)_4{\cdot}H_2O\}_n$ (**9**) which includes both polymeric and macrocyclic elements (Fig. 12). The $[Zn_2(C_{11}COO)_2(H_2O)_2]^{2+}$ unit has a discrete Zn_2L_2 macrocyclic structure, whereas the $[Zn_2(C_{11}COO)_2]^{2+}$ unit is a double stranded or 'ribbon' coordination polymer[2a] with carboxylate groups bridging a Zn_2 dimer. Both of the Zn^{II} centres in the discrete dimetallic macrocycle exhibit a ZnN_3O_3 octahedral geometry, with the third oxygen donor being an aqua ligand. Each Zn^{II} of the ribbon polymer displays a distorted square pyramidal geometry with a ZnN_3O_2 coordination environment (τ = 0.21 Zn3, 0.24 Zn4); the nitrogen atoms of the di(pyridylmethyl)amino group and one carboxylate oxygen atom occupy the equatorial sites, while an oxygen atom a second carboxylate ligand occupies the axial sites for each metal. The polymer can alternatively be described as Zn_2L_2 macrocycles, as was seen for **8**, linked *via* the second carboxylate oxygen that ligates the neighbouring Zn^{II} centre. It is noted that all O–Zn bonds for the bridging carboxylates fall within the range 2.009(3)–2.056(3) Å, indicative of a relatively symmetrical binding mode.

The discrete metallomacrocycles sit across the polymeric ribbon in a crossed "X-like" orientation (Fig. 13 and 14) as is seen for the macrocyclic structure **8**. Following the trend seen for the macrocyclic structures with aqua ligands, the hydrogen atoms of the water ligands in **9** interact with a neighbouring carbonyl oxygen. The pair of hydrogen bonds (O13–H132···O21 1.86(5) Å and O23–H231···O11 1.82(4) Å, dashed orange lines, Fig. 13) at each end of the macrocycle are relatively short and strong, and give rise to H-bonded ribbons of macrocycles (blue, Fig. 14) that weave through the coordination polymer chains (red). The second hydrogen of the aqua ligands is donated to a perchlorate oxygen atom (O13–H131···O83 2.04(4) Å and O23–H232···O72 2.08(4) Å, dashed blue lines, Fig. 13). These hydrogen bond distances are typical of their respective types.[27] The nanosegregation of the aromatic and aliphatic regions of the ligands is illustrated in Fig. 15; the pyridyl/ionic domains are highlighted in blue and the crossed alkyl domain in yellow.

Alkyl chain conformation

As the length of the alkyl chain increases, the number of potential conformations grows exponentially giving access to widening range of coordination polymers on moving from C_3COOH to $C_{11}COOH$. The conformation about the *n*-1 carbon–carbon bonds in the alkyl backbone may be characterised as *trans*/*anti* (T, torsion angle *ca.* 180°) or gauche (G),[6a,30] and the ligand conformation of each independent C_nCOO^- ligand in **1–9** has been analysed (Table 2).

The lowest energy all-T conformation places the two metal binding sites at the greatest separation and it is the T arrangement that dominates in this series, especially in complexes of the longer ligands (**7–9**). The all-T chains pack efficiently side-by-side (as exemplified in Fig. 14 & 15) and the ligands of **7–9** exhibit, at most, one bond with a G conformation. Notably, where a ligand contains a G unit, it is the second C–C bond from the amine nitrogen and the partner

Table 2 Alkyl chain conformations of the carboxylate ligands in **1**–**9** and related structures with perchlorate anions

Ligand C_nCOO^-	Alkyl linker conformation (OOC → N_3)[a]	
n	M = Zn	M = Cu
3	GT (**1**)	GG (**4**)
	GT (CSD: YACYUK)[8e]	TT (CSD: EYEHAR)[8c]
4	TTT [all ligands] (**2**)	TGT [both ligands] (**5**)
		TGT (CSD: NEDSEV)[8b]
5	TTTT (**3**)	TGTT (**6**)
	TTTT (CSD: HAYXIP)[8d]	TTTT (CSD: NEDSIZ)[8b]
7	TTGTTT (**7**)	
10	TTTTTTTGT [Zn1, Zn3] (**8**)	
	TTTTTTTTT [Zn2, Zn4]	
11	TTTTTTTTGT [Zn1, Zn2] (**9**)	
	TTTTTTTTTT [Zn3, Zn4]	

[a] T = *trans* (*anti*), G = gauche.

ligand in the macrocycle also exhibits a G unit in the same position giving rise to a (pseudo)symmetrical arrangement (Zn1/Zn3 in **8**, Zn1/Zn2 in **9**).

The unusual folded back binding mode of the carboxylate in **4** results in a GG conformation of the propylene alkyl linker to the bis(2-pyridylmethyl)amino head group (Fig. 5a). The related structure of the same carboxylate ligand[8c] possess a TT conformation propylene chain (Fig. 5b) with a significantly greater Cu···Cu separation (9.370(1) *vs.* 4.4251(7) Å in **4**).

Conclusions

The reaction of $M(ClO_4)_2{\cdot}6H_2O$ (M = Zn^{II} or Cu^{II}) with unsymmetrical, ditopic di(pyridylmethyl)amino carboxylate ligands (**C_nCOOH**) affords species with a 1 : 1 metal–ligand ratio, both in solution phase and solid-state studies. Reaction conditions (solvents, temperature, concentrations) were kept consistent throughout crystal growth experiments, the only variable being the number of methylene units in the alkyl linker thus allowing the effect of the alkyl chain to be probed. It is apparent that the alkyl linker length has an impact on solid-state coordination topologies with **C_nCOOH**, ranging from 1D coordination polymers to metallomacrocycles.

Six coordination polymers of short alkyl chain ligands (**C_nCOOH**, $n \leq 5$; Zn^{II} complexes: **1**–**3** and Cu^{II} complexes: **4**–**6**) were isolated and investigated by X-ray crystallography. Of note is the Zn^{II} coordination polymer **1** (n = 3) which displays intramolecular hydrogen bonding that leads to a wave topology, whereas the Cu^{II} coordination polymer **4** of the same ligand has an unusual polymeric structure where a carboxylate oxygen atom bridges two Cu^{II} metal centres of the polymer backbone. The carboxylate ligand in **4** folds back in a "scorpion-like" fashion giving rise to mini cyclic subunits along the polymeric chain. The presence of a methanol solvate molecule appears crucial in the constitution of **4** as a more conventional polymeric structure with lattice water molecules is obtained when other crystallisation solvents are utilised.[8c]

Novel head-to-tail Zn^{II} macrocycles were formed from the longer alkyl chain ligands (**C_nCOOH**, $n \geq 7$). Crystal structures **7**–**9** display intriguing coordination architectures: a discrete Zn_2L_2 metallomacrocycle (**7**, n = 7), four independent Zn_2L_2 macrocycles that arrange themselves into interlocked stacks (**8**, n = 10), and a tightly woven network consisting of macrocycles, linked by hydrogen and coordinate bonds along the *a*- and *c*-axes, respectively (**9**, n = 11). Note that metallomacrocycles are only observed with the longer alkyl chain ligands, and this behaviour is accompanied by a shift in N_3 coordination geometry of the di(pyridylmethyl)-amino head group from meridional in the short polymers to facial in the macrocycles (n = 7, 10). In all cases the perchlorate anions are non-coordinating and are thought to have minimal effect of the coordination topology.[31] It appears that the longer alkyl chain linkers, by virtue of their greater conformational freedom and ability to engage in efficient close packing with each other in the solid-state, give rise to entropically-favoured macrocyclic coordination topologies. For n = 7 and 10, macrocycle formation is accompanied by a facial arrangement of the N_3-donors, but for n = 11 a geometry closer to meridional is now possible without compromising steric hindrance or packing effects. The short linkers are not able to stabilise M_2L_2 macrocycles due to steric constraints, and in the absence of mitigating intermolecular interactions in the solid-state, adopt the expected catenated structures.

Acknowledgements

K.R. is grateful to Mahidol Wittayanusorn School (MWITS) and the Royal Thai government for financial support, and the University of Otago for a doctoral scholarship. Data for one structure were obtained on the MX2 beamline at the Australian Synchrotron, Victoria, Australia.

Notes and references

1 (*a*) A. Jana and S. Mohanta, *CrystEngComm*, 2014, **16**, 5494–5515; (*b*) K. Zhang, C. Jin, Y. Sun, F. Chang and W. Huang, *Inorg. Chem.*, 2014, **53**, 7803–7805; (*c*) D. Liu, J.-P. Lang and B. F. Abrahams, *Chem. Commun.*, 2013, **49**, 2682–2684; (*d*) O. Chepelin, J. Ujma, X. Wu, A. M. Z. Slawin, M. B. Pitak, S. J. Coles, J. Michel, A. C. Jones, P. E. Barran and P. J. Lusby, *J. Am. Chem. Soc.*, 2012, **134**, 19334–19337; (*e*) A. Goswami, S. Sengupta and R. Mondal, *CrystEngComm*, 2012, **14**, 561–572; (*f*) Y.-L. Wang, J.-H. Fu, Y.-L. Jiang, Y. Fu, W.-L. Xiong and Q.-Y. Liu, *CrystEngComm*, 2012, **14**, 7245–7252; (*g*) X. Lv, L. Liu, C. Huang, L. A. Guo, J. Wu, H. Hou and Y. Fan, *Dalton Trans.*, 2014, **43**, 15475–15481; (*h*) M. Yoon, R. Srirambalaji and K. Kim, *Chem. Rev.*, 2011, **112**, 1196–1231.

2 (*a*) W. L. Leong and J. J. Vittal, *Chem. Rev.*, 2011, **111**, 688–764; (*b*) J. Cao, J.-C. Liu, W.-T. Deng, R.-Z. Li and N.-Z. Jin, *Electrochim. Acta*, 2013, **112**, 515–521; (*c*) P. Niranjana, A. Pati, S. K. Porwal, V. Ramkumar, S. J. Gharpure and D. K. Chand, *CrystEngComm*, 2013, **15**, 9623–9633; (*d*) A. Dorazco-Gonzalez, S. Martinez-Vargas, S. Hernandez-Ortega

and J. Valdes-Martinez, *CrystEngComm*, 2013, **15**, 5961–5968; (*e*) A. Beziau, S. A. Baudron, G. Rogez and M. W. Hosseini, *CrystEngComm*, 2013, **15**, 5980–5985; (*f*) X.-H. Chang, Y. Zhao, X. Feng, L.-F. Ma and L.-Y. Wang, *Polyhedron*, 2014, **83**, 159–166.

3 (*a*) A. Beheshti, W. Clegg, V. Nobakht and R. W. Harrington, *Polyhedron*, 2014, **81**, 256–260; (*b*) J. Wu, F. Pan, H. Hou, J. A. Zhao, Y. Zhao and Y. Fan, *Inorg. Chem. Commun.*, 2009, **12**, 750–754; (*c*) W. Meng, Y. Liu, Y. Zhao, H. Hou and Y. Fan, *Polyhedron*, 2013, **52**, 1219–1226; (*d*) Q.-G. Wang, Y.-S. Xie, F.-H. Zeng, S.-W. Ng and W.-H. Zhu, *Inorg. Chem. Commun.*, 2010, **13**, 929–931; (*e*) C. Chen, J. Zhang, G. Li, P. Shen, H. Jin and N. Zhang, *Dalton Trans.*, 2014, **43**, 13965–13971.

4 (*a*) T.-F. Liu, J. Lu and R. Cao, *CrystEngComm*, 2010, **12**, 660–670; (*b*) Y. J. Lee and S. W. Lee, *Polyhedron*, 2013, **53**, 103–112; (*c*) J. M. Ellsworth and H.-C. zur Loye, *Dalton Trans.*, 2008, 5823–5835; (*d*) S. Gao, R.-Q. Fan, L.-S. Qiang, P. Wang, S. Chen, X.-M. Wang and Y.-L. Yang, *CrystEngComm*, 2014, **16**, 1113–1125; (*e*) H. Arora, F. Lloret and R. Mukherjee, *Eur. J. Inorg. Chem.*, 2009, 3317–3325; (*f*) M. Paul and P. Dastidar, *CrystEngComm*, 2014, **16**, 7815–7829; (*g*) L. Carlucci, G. Ciani, D. M. Proserpio and S. Rizzato, *CrystEngComm*, 2003, **5**, 190–199; (*h*) L. Carlucci, G. Ciani, M. Moret, D. M. Proserpio and S. Rizzato, *Chem. Mater.*, 2002, **14**, 12–16.

5 G. Ambrosi, M. Formica, V. Fusi, L. Giorgi, A. Guerri, S. Lucarini, M. Micheloni, P. Paoli, P. Rossi and G. Zappia, *Inorg. Chem.*, 2005, **44**, 3249–3260.

6 (*a*) P.-C. Cheng, P.-T. Kuo, M.-Y. Xie, W. Hsu and J.-D. Chen, *CrystEngComm*, 2013, **15**, 6264–6272; (*b*) Y.-Q. Huang, Z.-L. Shen, X.-Y. Zhou, T.-a. Okamura, Z. Su, J. Fan, W.-Y. Sun, J.-Q. Yu and N. Ueyama, *CrystEngComm*, 2010, **12**, 4328–4338; (*c*) A. Almesaker, S. A. Bourne, G. Ramon, J. L. Scott and C. R. Strauss, *CrystEngComm*, 2007, **9**, 997–1010.

7 H. Arora and R. Mukherjee, *New J. Chem.*, 2010, **34**, 2357–2365.

8 (*a*) M. Bartholomä, B. Ploier, H. Cheung, W. Ouellette and J. Zubieta, *Inorg. Chim. Acta*, 2010, **363**, 1659–1665; (*b*) K.-Y. Choi, S.-Y. Park, Y.-M. Jeon and H. Ryu, *Struct. Chem.*, 2005, **16**, 649–656; (*c*) K.-Y. Choi, Y.-M. Jeon, H. Ryu, J.-J. Oh, H.-H. Lim and M.-W. Kim, *Polyhedron*, 2004, **23**, 903–911; (*d*) K.-Y. Choi, H. Ryu, J. Ko, S. O. Kang, W.-S. Han and I.-H. Suh, *Acta Crystallogr., Sect. E: Struct. Rep. Online*, 2005, **61**, m2474–m2476; (*e*) K.-Y. Choi and Y.-M. Jeon, in *Main Group Metal Chemistry*, 2003, vol. 26, p. 313.

9 A. I. Buvailo, E. Gumienna-Kontecka, S. V. Pavlova, I. O. Fritsky and M. Haukka, *Dalton Trans.*, 2010, **39**, 6266–6275.

10 (*a*) E. C. Constable, K. Harris, C. E. Housecroft and M. Neuburger, *Dalton Trans.*, 2011, **40**, 1524–1534; (*b*) X.-L. Tang, W. Dou, J.-a. Zhou, G.-L. Zhang, W.-S. Liu, L.-Z. Yang and Y.-L. Shao, *CrystEngComm*, 2011, **13**, 2890–2898; (*c*) Q.-X. Liu, X.-Q. Yang, X.-J. Zhao, S.-S. Ge, S.-W. Liu, Y. Zang, H.-b. Song, J.-H. Guo and X.-G. Wang, *CrystEngComm*, 2010, **12**, 2245–2255; (*d*) H. S. Chow, E. C. Constable, C. E. Housecroft, M. Neuburger and S. Schaffner, *Polyhedron*, 2006, **25**, 1831–1843.

11 (*a*) B. K. Tripuramallu, P. Manna and S. K. Das, *CrystEngComm*, 2014, **16**, 10300–10308; (*b*) E. Guzmán-Percástegui, L. N. Zakharov, J. G. Alvarado-Rodríguez, M. E. Carnes and D. W. Johnson, *Cryst. Growth Des.*, 2014, **14**, 2087–2091; (*c*) S. Yamashita, M. Nihei and H. Oshio, *Chem. Lett.*, 2003, **32**, 808–809; (*d*) Y. Q. Zheng, J. Sun and Y. W. Fang, *Z. Kristallogr. - New Cryst. Struct.*, 2003, **218**, 221; (*e*) L. C. Nathan, J. E. Koehne, J. M. Gilmore, K. A. Hannibal, W. E. Dewhirst and T. D. Mai, *Polyhedron*, 2003, **22**, 887–894; (*f*) J. Guo, L. Zhang, H. Ma, Z. Chen, D. Sun, Y. Wei and D. Sun, *Inorg. Chem. Commun.*, 2013, **28**, 75–80.

12 *Compass V 1.3*, Bruker Daltronics, Bremen, Germany.

13 T. M. McPhillips, S. E. McPhillips, H.-J. Chiu, A. E. Cohen, A. M. Deacon, P. J. Ellis, E. Garman, A. Gonzalez, N. K. Sauter, R. P. Phizackerley, S. M. Soltis and P. Kuhn, *J. Synchrotron Radiat.*, 2002, **9**, 401–406.

14 *APEX2, SAINT, XPREP*, (2009) Bruker AXS Inc., Madison, WI, USA.

15 *CrysAlisPro*, (2013) Agilent Technologies, Yarnton, Oxfordshire, UK.

16 W. Kabsch, *Acta Crystallogr., Sect. D: Biol. Crystallogr.*, 2010, **66**, 125–132.

17 R. C. Clark and J. S. Reid, *Acta Crystallogr., Sect. A: Found. Crystallogr.*, 1995, **51**, 887–897.

18 (*a*) G. M. Sheldrick, *SHELX-97 Programs for Crystal Structure Analysis*, (1998), Göttingen, Germany; (*b*) G. M. Sheldrick, *Acta Crystallogr., Sect. A: Found. Crystallogr.*, 2008, **64**, 112–122.

19 L. Palatinus and G. Chapuis, *J. Appl. Crystallogr.*, 2007, **40**, 786–790.

20 A. Altomare, M. C. Burla, M. Camalli, G. L. Cascarano, C. Giacovazzo, A. Guagliardi, A. G. G. Moliterni, G. Polidori and R. Spagna, *J. Appl. Crystallogr.*, 1999, **32**, 115–119.

21 (*a*) L. J. Barbour, *J. Supramol. Chem.*, 2001, **1**, 189–191; (*b*) L. J. Barbour, *X-Seed*, (2001).

22 F. J. Femia, K. P. Maresca, S. M. Hillier, C. N. Zimmerman, J. L. Joyal, J. A. Barrett, O. Aras, V. Dilsizian, W. C. Eckelman and J. W. Babich, *J. Nucl. Med.*, 2008, **49**, 970–977.

23 (*a*) J. B. Fenn, M. Mann, C. K. Meng, S. F. Wong and C. M. Whitehouse, *Mass Spectrom. Rev.*, 1990, **9**, 37–70; (*b*) R. Colton, A. D'Agostino and J. C. Traeger, *Mass Spectrom. Rev.*, 1995, **14**, 79–106; (*c*) W. Henderson, B. K. Nicholson and L. J. McCaffrey, *Polyhedron*, 1998, **17**, 4291–4313; (*d*) H. Lavanant, E. Hecquet and Y. Hoppilliard, *Int. J. Mass Spectrom.*, 1999, **185–187**, 11–23; (*e*) M. Yamashita and J. B. Fenn, *J. Phys. Chem.*, 1984, **88**, 4451–4459; (*f*) M. Yamashita and J. B. Fenn, *J. Phys. Chem.*, 1984, **88**, 4671–4675; (*g*) C. M. Whitehouse, R. N. Dreyer, M. Yamashita and J. B. Fenn, *Anal. Chem.*, 1985, **57**, 675–679; (*h*) T. D. Burns, T. G. Spence, M. A. Mooney and L. A. Posey, *Chem. Phys. Lett.*, 1996, **258**, 669–679; (*i*) V. Katta, S. K. Chowdhury and B. T. Chait, *J. Am. Chem. Soc.*, 1990, **112**, 5348–5349.

24 (*a*) C. Y. Huang, in *Methods in Enzymology*, ed. L. P. Daniel, Academic Press, 1982, vol. 87, pp. 509–525; (*b*) K. S. Klausen and F. J. Langmyhr, *Anal. Chim. Acta*, 1963, **28**, 335–340; (*c*)

B.-M. Kukovec, I. Kodrin, V. Vojković and Z. Popović, *Polyhedron*, 2013, **52**, 1349–1361.
25 K. Nakamoto, *Infrared and Raman Spectra of Inorganic and Coordination Compounds*, Sixth edn, John Wiley & Sons, Hoboken, NY, 2009.
26 A. W. Addison, T. N. Rao, J. Reedijk, J. van Rijn and G. C. Verschoor, *J. Chem. Soc., Dalton Trans.*, 1984, 1349–1356.
27 T. Steiner, *Angew. Chem., Int. Ed.*, 2002, **41**, 48–76.
28 A. L. Spek, *Acta Crystallogr., Sect. C: Struct. Chem.*, 2015, **71**, 9–18.
29 (*a*) J. McMurtrie and I. Dance, *CrystEngComm*, 2005, **7**, 216–229; (*b*) I. Dance, *Mol. Cryst. Liq. Cryst.*, 2005, **440**, 265–293; (*c*) I. Dance and M. Scudder, *J. Chem. Soc., Dalton Trans.*, 1998, 1341–1350.
30 L. Carlucci, G. Ciani, D. M. Proserpio and S. Rizzato, *CrystEngComm*, 2002, **4**, 121–129.
31 A previous study of shorter di(pyridylmethyl)amino carboxylate ligands using other counteranions, such as nitrate and sulfate, has shown that the anion plays a non-innocent role in the coordination chemistry: see ref. 8*a*.

